ACS Macro Letters

Letter

pubs.acs.org/macroletters

Crystallization-Induced Redox-Active Nanoribbons of Organometallic Polymers

Jialong Wu,[†] Lu-Tao Weng,[‡] Wei Qin,[§] Guodong Liang,*[,†] and Ben Zhong Tang*[,§]

[†]DSAP, PCFM and GDHPPC lab, School of Chemistry and Chemical Engineering, Sun Yat-Sen University, Guangzhou 510275, China

[‡]Materials Characterization and Preparation Facility, Department of Chemical and Biomolecular Engineering, The Hong Kong University of Science and Technology, Hong Kong, China

[§]HKUST-Shenzhen Research Institute, No. 9 Yuexing first RD, South Area, Hi-tech Park, Nanshan, Shenzhen, China 518057

Department of Chemistry, Institute for Advanced Study, Division of Biomedical Engineering and Institute of Molecular Functional Materials, The Hong Kong University of Science and Technology, Clear Water Bay, Kowloon, Hong Kong, China

Guangdong Innovative Research Team, SCUT-HKUST Joint Research Laboratory, State Key Laboratory of Luminescent Materials and Devices, South China University of Technology, Guangzhou 510640, China

Supporting Information

ABSTRACT: Polymer/inorganic functional nanostructures are essential for the fabrication of high-performance nanodevices in the future. The synthesis of hybrid nanostructures is hindered by complicated synthetic protocols or harsh conditions. Herein, we report a facile and scalable method for the synthesis of organometallic polymer nanoribbons through crystallization of polymers capped with a ferrate complex. Nanoribbons consisted of a single crystalline polymer lamella coated with a redox-active ferrate complex on both sides. The nanoribbons had a width of approximately 70 nm and a thickness of 10 nm. With the merit of highly ordered crystalline structures of polymers and functional coating layers, as well as a highly anisotropic nature, the nanoribbons are useful in nanodevices and biosensors.

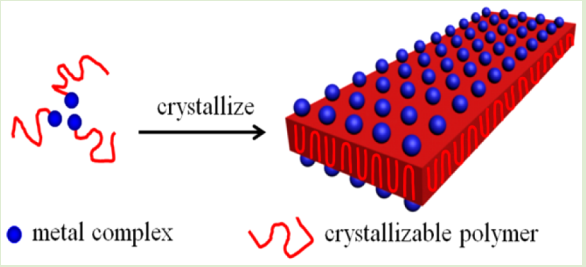

Highly anisotropic nanomaterials such as one-dimensional nanoribbons are crucial as building blocks for the fabrication of nanodevices with high performances.[1] For instance, electrically conductive nanoribbons are identified as connecting cables in nanodevices in the future.[2] In the past few decades, the synthesis of inorganic nanomaterials such as carbon nanotubes and gold nanowires through chemical vapor deposition or hydrothermal technique have been extensively investigated.[3] In contrast, there are limited works on the synthesis of polymer/inorganic hybrid nanostructures. In this regard, hybrid nanomaterials combine synergistically the inherent properties of their parent constituents and generate new functions to meet demands in engineering sectors. However, it is difficult to synthesize polymer-based nanomaterials with desirable compositions and structures through conventional approaches due to harsh synthetic conditions such as high temperature rendering the polymer to decompose during synthesis.

Self-assembly of polymers is emerging as a versatile approach for synthesis of hybrid nanomaterials.[4] Polymers with multiple components and functional units self-assemble into nanostructures with functional units-enriched nanodomains in bulk or solution.[5] Self-assembly of polymers can be regulated by the rational design of polymers, affording access to nanomaterials with multiple components and controlled morphologies. Manners and co-workers have synthesized cylindrical micelles with iron-enriched cores by living self-assembly of poly(ferrocenyldimethylsilane) based copolymers.[6] Self-assembly of cyanoferrate-containing amphiphilic block copolymers and subsequent coordination of cyanoferrate with Fe^{3+} ions resulted in polymer/Prussian blue hybrid nanostructures for drug encapsulation and controlled release applications.[7] In addition, postfunctionalization of self-assembled particles of block copolymers using functional nanoparticles is an alternative approach to hybrid nanostructures with internal nanophases. A variety of nanoparticles, including gold, titania, fullerence, and silica, have been incorporated into polymer matrices with controlled locations for energy applications.[8] Although these techniques enable access to hybrid nanostructures with controllable morphologies, they involve the use of block polymers. Complicated synthetic protocols and the availability of proper block copolymers limited the synthesis of hybrid nanomaterials and their applications in engineering sectors.

Received: March 12, 2015
Accepted: April 28, 2015
Published: May 7, 2015

DOI: 10.1021/acsmacrolett.5b00180
ACS Macro Lett. 2015, 4, 593−597

Developing new strategies for facile and scalable synthesis of hybrid nanomaterials is highly desirable.

Crystallization is a naturally occurring self-assembly process.[9] Macromolecular chains fold back and forth to form lamellae during crystallization, which offers a new opportunity for synthesis of anisotropic nanomaterials. Closely packed polymer chains endow the ultimate materials with advanced properties such as superior reduction in gas permeability compared to their amorphous counterparts.[10] Polymer crystals grow in two-dimensional directions to form infinite lamellae with a thickness of approximately 10 nm.[11] Such polymer lamellae with given thickness are promising materials for the fabrication of nanostructures. The problem lies in how to control the growth of crystals to form nanostructures with defined shapes. Herein, we reported a facile approach to control crystallization of polymers. We demonstrated that capping of crystallizable polymers with a metal complex resulted in the formation of nanoribbons of 70 nm in width and several microns in length during crystallization, as illustrated in Scheme 1. The functional

Scheme 1. Schematic Illustration of Crystallization-Induced Organometallic Polymer Nanoribbons

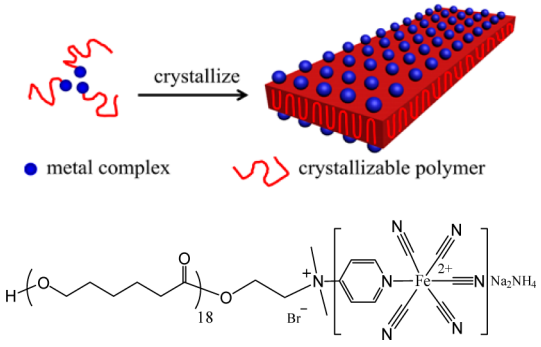

metal complex was expelled out of polymer crystals during crystallization and located on the surface. The approach possesses the following overwhelming advantages: (1) simple and easy synthesis protocols of end-functionalized homopolymers, evading block copolymers synthesized through harsh and fussy sequent living polymerization procedures; (2) surface-enriched metal complex layers endow nanomaterials designable functionalities; (3) synergistic integration of fabrication and functionality processes, avoiding postfunctionality process. With the above-mentioned merits, such crystallization-induced organometallic nanoribbons offer a new opportunity for the synthesis of highly anisotropic crystalline nanomaterials.

To synthesize polymer nanoribbons, poly(ε-caprolactone) monoterminated with pentacyano(4-(dimethylamino) pyridine) ferrate) (PCL-Fe, number-average molecular weight of PCL used was 2000 g/mol, see Supporting Information (SI), Figures S1−S6) in anhydrous tetrahydrofuran (THF; 0.5 mg/mL) was spin-coated onto clean mica wafers at 900 rpm for 15 s, followed by 3000 rpm for 60 s at room temperature. The fresh polymer films were annealed in vacuum at 40 °C for 12 h to allow PCL-Fe to crystallize.

Morphology of PCL-Fe was characterized using tapping mode atomic force microscopy (AFM) and transmission electron microscopy (TEM). AFM images showed that PCL-Fe formed nanoribbons of 70 nm in width and several microns in length (Figure 1A). The nanoribbons entangled together to

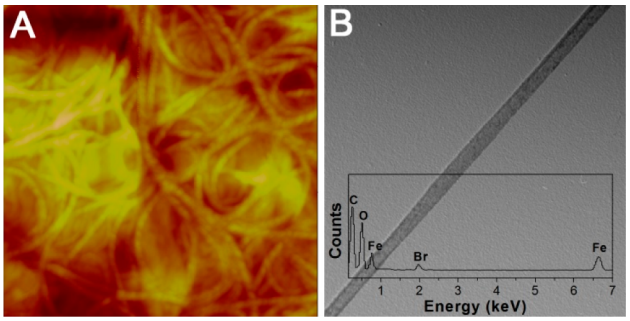

Figure 1. (A) AFM image (image size: 2.5 × 2.5 μm^2) and (B) TEM image of polymer nanoribbons. Inset is the EDX spectrum obtained from image (B).

form grains. The thickness of nanoribbons was estimated to be approximately 10 nm, suggesting that nanoribbons consisted of a single lamella. TEM images further confirmed the formation of nanoribbons (Figures 1B and S7). Effort to acquire TEM images at higher magnitude and elemental mapping was unsuccessful due to melting and decomposition of polymer nanoribbons upon exposure to intense electron bombardment. The EDX spectrum of the nanoribbons confirmed the presence of an iron element.

Surface composition of PCL-Fe nanoribbons was analyzed using time-of-flight secondary ion mass spectrometry (TOF-SIMS), which typically provides the surface composition of the outermost 1−2 nm of a sample.[12] As shown in Figure 2A, the

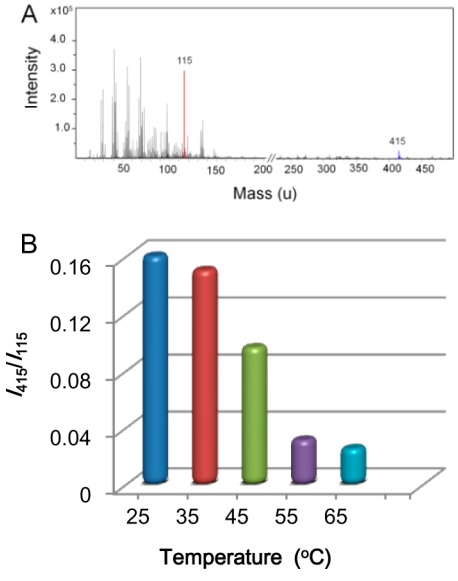

Figure 2. (A) Positive TOF-SIMS spectrum of PCL-Fe nanoribbons using Bi_3^+ as primary ion beam and (B) TOF-SIMS intensity ratio (I_{415}/I_{115}) of PCL-Fe nanoribbons as a function of temperature.

positive TOF-SIMS spectrum of PCL-Fe nanoribbons was composed of the fragments from both PCL backbones and end groups of ferrate complex. In particular, the fragment at m/z = 115 ($C_6H_{11}O_2^+$) represented the repeat units of PCL, while the fragment at m/z = 415 ($C_{14}H_{17}FeN_8Na_2O^+$) was ascribed to the ferrate complex (Table S3). This result was in good agreement with the chemical structure of PCL-TPE (Scheme 1).

In order to determine whether the ferrate complex was on the surface, two different experimental approaches were

DOI: 10.1021/acsmacrolett.5b00180
ACS Macro Lett. 2015, 4, 593−597

used.[11a] The first approach was to compare the relative intensity of the end group versus the PCL repeat unit at different sampling depths, which could be realized using two different primary ion beams (Bi_3^+ and C_{60}^+). This is because the sampling depth is dependent on the size of primary ion beams under identical ion dosage, and a smaller size ion beam provides a deeper sampling depth.[12a,b] For the PCL-Fe nanoribbons, the TOF-SIMS intensity ratio between the peak at m/z = 415 and that at m/z = 115 (I_{415}/I_{115}) was 5.3 × 10^{-2} when using smaller Bi_3^+ ions as the primary ion beam, which was only 1/3 of that using bigger C_{60}^+ ions as the primary ion beam (16 × 10^{-2}). This showed that ferrate complex fraction decreased drastically with increasing sampling depth, revealing that ferrate complex moieties were located on the surface of PCL-Fe nanoribbons.

The second approach was to compare the surface composition of PCL-Fe nanoribbons at various temperatures using C_{60}^+ as the primary ion beam. As displayed in Figure 2B, the intensity ratio I_{415}/I_{115} started to decrease from 35 °C and decreased abruptly after the melting temperature of PCL-Fe (49.2 °C). At 65 °C, the intensity ratio was only 1/6 of that obtained on PCL-Fe nanoribbons (25 °C). Since PCL-Fe was thermostable and did not decompose at 65 °C (Figure S6),[13] it is expected that at 65 °C the PCL-Fe lamellae were melted and the end groups of the ferrate complex were randomly distributed across the whole polymer film.[12b] As a result, the surface ferrate complex concentration at the molten state is much lower compared to that of nanoribbons. Based on the TOF-SIMS results, the grafting density of ferrate complex moieties was estimated to be 5.4 × 10^{17} m^{-2}, and the coverage ratio of the ferrate complex on PCL-Fe nanoribbons was 10.3% (SI).

The TOF-SIMS results suggest that the end groups of ferrate are expelled out of PCL crystals during the crystallization of PCL segments. This results in ferrate moieties coating on the surface due to tethering to polymers. Two possible reasons are considered: (1) size mismatch between of ferrate moieties and PCL crystal cell[14] (Schemes S1 and S2, SI); (2) low miscibility between chemically distinct composition of PCL and ferrate complex. Moreover, it has been reported that small end groups such as thiol, hydroxide, carboxyl acid, and benzyl were excluded from crystal cell of polymers and are finally located on the surface.[15] Ferrate moieties are much larger than these groups and should have a higher chance to locate on the surface of PCL-Fe crystals, as schematically illustrated in Scheme 1.

We monitored the morphological evolution of PCL-Fe during annealing. Fresh PCL-Fe films showed lamellar structures, as shown in Figure 3A. Surface of polymer films roughened obviously and granular grains formed when annealing the fresh films at 40 °C for 4 h. Further annealing for 8 h led to the appearance of nanoribbons with a width of 70 nm. After annealing for 12 h, lamellar structures completely disappeared and nanoribbons with uniform width formed. In fresh PCL-Fe films prepared by spin coating, PCL macromolecules mainly existed as amorphous coils due to rapid evaporation of solvent. Annealing of PCL-Fe films initiates crystallization of PCL, accompanied by the formation of nanoribbons.

Crystallization of PCL-Fe during annealing was followed using polarizing optical microscopy (POM; Figure 4). POM images of fresh films showed isolated bright dots throughout observation field, implying less ordered structures of nascent PCL-Fe films due to low crystallinity. Fan-like bright motifs

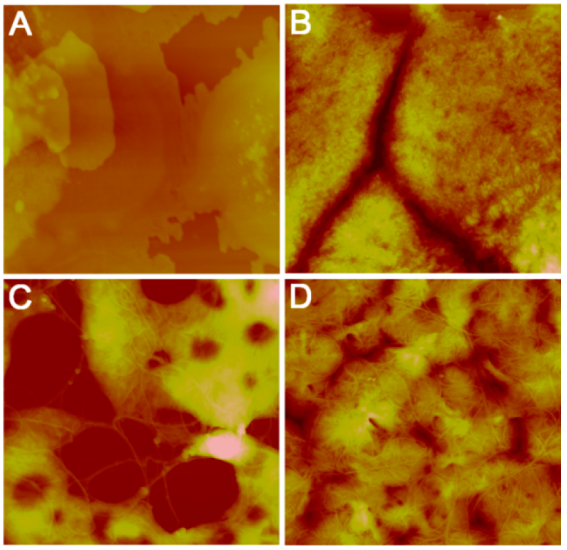

Figure 3. AFM images of polymer nanoribbons annealed for various times (A) 0, (B) 4, (C) 8, and (D) 12 h. Image size: 10 × 10 μm^2.

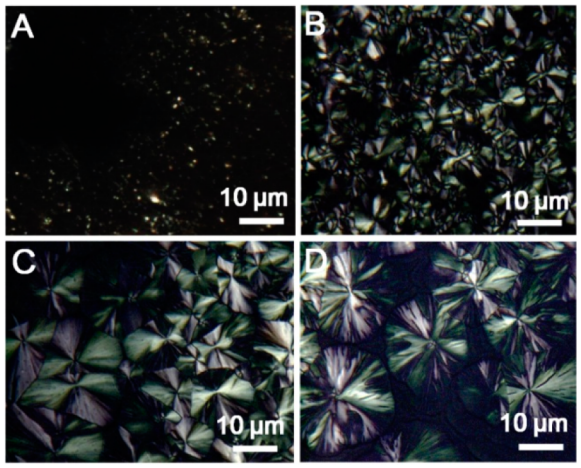

Figure 4. Polarizing optical microscopy (POM) images of PCL-Fe films annealed for various durations (A) 0, (B) 4, (C) 8, and (D) 12 h.

were observed for PCL-Fe films annealed for 4 h. Annealing for 8 h gave rise to larger fan-like patterns. Further annealing for 12 h led to the formation of perfect spherulites. This verified that crystallinity of PCL-Fe films was significantly enhanced during annealing treatment.

Microstructures of nanoribbons were further investigated using XRD. XRD spectrum of PCL-Fe nanoribbons showed two distinct diffraction peaks at 21.3° and 23.6° associated with (110) and (200) diffraction plane of PCL orthorhombic crystals, respectively, confirming that PCL crystallized (Figure S9, SI). In contrast, fresh PCL-Fe showed a broad and weak peak at 21.3° and 23.6°, respectively, indicating low crystallinity of fresh PCL-Fe films.

To understand the formation of PCL-Fe nanoribbons, in a control experiment, morphology of unmodified PCL2k was investigated. Not ribbon-like, but lamellar morphology was observed for PCL2k (Figure S10, SI). It is apparent that the distinct difference in morphology between PCL and PCL-Fe is derived from end-capping of PCL with ferrate complex. For PCL-Fe, negatively charged ferrate is expelled out of polymer lamellar crystals and resides on the surface during crystallization

DOI: 10.1021/acsmacrolett.5b00180
ACS Macro Lett. 2015, 4, 593−597

of PCL macromolecules. We believe that the charge distribution on the surface of PCL crystals is different along different directions, leading to different growth rates of the PCL, thus, nanoribbons, instead of common hexagonal PCL single crystals, are formed. When a certain amount of ferrate gathers on the surface, accumulated charge prevents uncrystallized PCL-Fe from attaching to crystalline site to some extent due to electrostatic repulsion. Moreover, the steric effect of bulky ferrate complex also hinders the diffusion of PCL-Fe macromolecules toward crystalline sites. The balance between driving force of crystallization and repulsing force including electrostatic interaction and steric effect leads to the formation of nanoribbons with given width.

To further confirm the above conclusion, neutral tetraphenylethene was used to cap PCL (PCL-TPE, Scheme S3, Figure S11, SI). Not ribbons, but lamellae were observed for PCL-TPE, as expected. This further verified that charged ferrate complex is crucial for the formation of ribbons. The nature of polymer backbone also plays a role in the formation of ribbons. Polyethylene capped with ferrate complex (PE-Fe, Scheme S4, Figure S12, SI) formed tiny flowers consisted of lamellae possibly due to strong crystallizability of polyethylene compared to PCL.[13b]

We investigated the effect of ferrate fractions on morphology of PCL-Fe. Ferrate fractions of PCL-Fe were regulated by changing molecular weight of PCL. PCL-Fe with higher molecular weights of PCL means lower ferrate fractions since ferrate complex is an end group (Table S1, SI). AFM images (Figure 5) showed that PCL-Fe with PCL molecular weight of

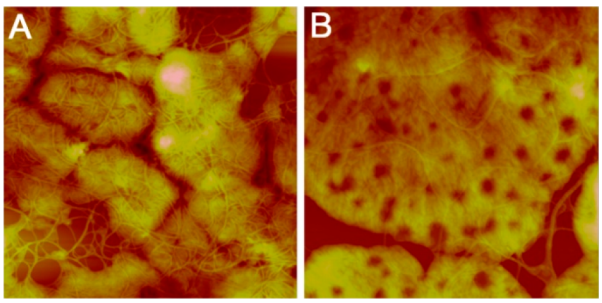

Figure 5. AFM images of PCL-Fe with various molecular weights (A) 5 and (B) 10 kg/mol. Image size: 10 × 10 μm^2.

5 kg/mol (PCL5k-Fe) also formed nanoribbons of 70 nm in width. Further increasing molecular weight of PCL to 10 kg/mol, PCL10k-Fe formed lamellae together with a small portion of nanoribbons. Interestingly, the width of nanoribbons remained unchanged (approximately 70 nm) regardless of molecular weight of PCL-Fe. This facilitates the synthesis of nanoribbons in engineering sectors. PCL-Fe with various molecular weights (PCL2k-Fe, PCL5k-Fe, and PCL10k-Fe) exhibited similar crystallinity (46.5, 49.5, and 46.5%, respectively, SI, Table S2), showing comparable driving force. On the other hand, repulsing force including electrostatic interaction and steric effect associated with ferrate complex was also similar for PCL-Fe with various molecular weights. Thus, nanoribbons with similar width were formed for PCL-Fe, independent of molecular weight of PCL-Fe. For PCL-Fe with high molecular weight (i.e., PCL10k-Fe), parts of PCL segments together with ferrate complex formed nanoribbons, while another extra PCL segments formed lamellae. Thus, both nanoribbon and lamellae formed for PCL-Fe with high molecular weight (PCL10k-Fe).

Given the surface-enriched ferrate complex in PCL-Fe nanoribbons, we investigated their electrochemical behavior using cyclic voltammetry (CV). A typical CV curve for PCL-Fe nanoribbons showed a set of distinct redox pair at $E_{1/2}$ = 0.084 V with a peak separation of 167 mV, ascribed to Fe(II)/Fe(III) transition (Figure S13, SI).[16] This verified the formation of regular ferrate layers through nanoribbons. For purpose of comparison, CV curve for as-cast PCL-Fe films was also scanned under identical conditions. A pair of weak redox peaks was recognized. Compared with as-cast PCL-Fe films, nanoribbons exhibited 5-fold peak current. Such significantly enhanced peak current is likely due to surface-enriched ferrate in PCL-Fe nanoribbons.

In summary, organometallic polymer nanoribbons have been successfully synthesized through crystallization of ferrate-capped polymers. Nanoribbons consisted of a single crystalline polymer lamella coated with redox-active ferrate complex on both sides. The nanoribbons had a width of approximately 70 nm and thickness of 10 nm. The nanoribbons were electrochemically active. Given facile and scalable synthetic procedures, surface-enriched functional layers and closely packed crystalline structures of the nanoribbons, the crystallization-induced organometallic polymer nanoribbons offers new opportunity for facile and scalable synthesis of highly anisotropic functional nanomaterials.

■ ASSOCIATED CONTENT

Supporting Information

XRD curves of PCL-Fe, TEM image, and the synthesis of PCL-Fe. The Supporting Information is available free of charge on the ACS Publications website at DOI: 10.1021/acsmacrolett.5b00180.

■ AUTHOR INFORMATION

Corresponding Authors

*E-mail: lgdong@mail.sysu.edu.cn.
*E-mail: tangbenz@ust.hk.

Notes

The authors declare no competing financial interest.

■ ACKNOWLEDGMENTS

The financial support is partially from NSFC (21074151 and 21374136).

■ REFERENCES

(1) (a) Baringhaus, J.; Ruan, M.; Edler, F.; Tejeda, A.; Sicot, M.; Taleb-Ibrahimi, A.; Li, A. P.; Jiang, Z. G.; Conrad, E. H.; Berger, C.; Tegenkamp, C.; de Heer, W. A. *Nature* **2014**, *506*, 349−354. (b) Palacios, J. J. *Nat. Phys.* **2014**, *10*, 182−183.

(2) Wang, X. R.; Ouyang, Y. J.; Jiao, L. Y.; Wang, H. L.; Xie, L. M.; Wu, J.; Guo, J.; Dai, H. J. *Nat. Nanotechnol.* **2011**, *6*, 563−567.

(3) (a) Peng, X. H.; Chen, J. Y.; Misewich, J. A.; Wong, S. S. *Chem. Soc. Rev.* **2009**, *38*, 1076−1098. (b) Lal, S.; Hafner, J. H.; Halas, N. J.; Link, S.; Nordlander, P. *Acc. Chem. Res.* **2012**, *45*, 1887−1895.

(4) (a) Orilall, M. C.; Wiesner, U. *Chem. Soc. Rev.* **2011**, *40*, 520−535. (b) Schacher, F. H.; Rupar, P. A.; Manners, I. *Angew. Chem., Int. Ed.* **2012**, *51*, 7898−7921. (c) Whittell, G. R.; Manners, I. *Adv. Mater.* **2007**, *19*, 3439−3468.

(5) (a) Hu, J. M.; Wu, T.; Zhang, G. Y.; Liu, S. Y. *J. Am. Chem. Soc.* **2012**, *134*, 7624−7627. (b) Liu, Y. J.; Li, Y. C.; He, J.; Duelge, K. J.; Lu, Z. Y.; Nie, Z. H. *J. Am. Chem. Soc.* **2014**, *136*, 2602−2610. (c) Liang, G. D.; Ni, H.; Bao, S. P.; Zhu, F. M.; Gao, H. Y.; Wu, Q.;

DOI: 10.1021/acsmacrolett.5b00180
ACS Macro Lett. 2015, 4, 593−597

Tang, B. Z. *Langmuir* **2014**, *30*, 6294−6301. (d) Liang, G. D.; Ni, H.; Bao, S. P.; Zhu, F. M.; Gao, H. Y.; Wu, Q. *J. Phys. Chem. B* **2014**, *118*, 6339−6345.
(6) (a) Rupar, P. A.; Chabanne, L.; Winnik, M. A.; Manners, I. *Science* **2012**, *337*, 559−562. (b) Wang, X. S.; Liu, K.; Arsenault, A. C.; Rider, D. A.; Ozin, G. A.; Winnik, M. A.; Manners, I. *J. Am. Chem. Soc.* **2007**, *129*, 5630−5639. (c) Wang, X. S.; Guerin, G.; Wang, H.; Wang, Y. S.; Manners, I.; Winnik, M. A. *Science* **2007**, *317*, 644−647.
(7) (a) Roy, X.; Hui, J. K. H.; Rabnawaz, M.; Liu, G. J.; MacLachlan, M. J. *J. Am. Chem. Soc.* **2011**, *133*, 8420−8423. (b) Roy, X.; Hui, J. K. H.; Rabnawaz, M.; Liu, G. J.; MacLachlan, M. J. *Angew. Chem., Int. Ed.* **2011**, *50*, 1597−1602. (c) Liang, G. D.; Xu, J. T.; Wang, X. S. *J. Am. Chem. Soc.* **2009**, *131*, 5378−5379. (d) Liu, Y. B.; Wang, X. S. *Polym. Chem.* **2012**, *3*, 2632−2639. (e) Ye, S. J.; Liu, Y. B.; Chen, S. J.; Liang, S.; McHale, R.; Ghasdian, N.; Lu, Y.; Wang, X. S. *Chem. Commun.* **2011**, *47*, 6831−6833. (f) McHale, R.; Ghasdian, N.; Liu, Y. B.; Ward, M. B.; Hondow, N. S.; Wang, H. H.; Miao, Y. Q.; Brydson, R.; Wang, X. S. *Chem. Commun.* **2010**, *46*, 4574−4576. (g) McHale, R.; Ghasdian, N.; Liu, Y. B.; Wang, H. H.; Miao, Y. Q.; Wang, X. S. *Macromol. Rapid Commun.* **2010**, *31*, 856−860.
(8) (a) Kim, M. P.; Kang, D. J.; Jung, D. W.; Kannan, A. G.; Kim, K. H.; Ku, K. H.; Jang, S. G.; Chae, W. S.; Yi, G. R.; Kim, B. J. *ACS Nano* **2012**, *6*, 2750−2757. (b) Wei, Q. S.; Lin, Y.; Anderson, E. R.; Briseno, A. L.; Gido, S. P.; Watkins, J. J. *ACS Nano* **2012**, *6*, 1188−1194. (c) Connal, L. A.; Lynd, N. A.; Robb, M. J.; See, K. A.; Jang, S. G.; Spruell, J. M.; Hawker, C. J. *Chem. Mater.* **2012**, *24*, 4036−4042. (d) Docampo, P.; Guldin, S.; Stefik, M.; Tiwana, P.; Orilall, M. C.; Huttner, S.; Sai, H.; Wiesner, U.; Steiner, U.; Snaith, H. J. *Adv. Funct. Mater.* **2010**, *20*, 1787−1796. (e) Lin, Y.; Lim, J. A.; Wei, Q. S.; Mannsfeld, S. C. B.; Briseno, A. L.; Watkins, J. J. *Chem. Mater.* **2012**, *24*, 622−632. (f) Kao, J.; Thorkelsson, K.; Bai, P.; Rancatore, B. J.; Xu, T. *Chem. Soc. Rev.* **2013**, *42*, 2654−2678.
(9) (a) Kim, Y. J.; Cho, C. H.; Paek, K.; Jo, M.; Park, M. K.; Lee, N. E.; Kim, Y. J.; Kim, B. J.; Lee, E. *J. Am. Chem. Soc.* **2014**, *136*, 2767−2774. (b) Qian, J. S.; Li, X. Y.; Lunn, D. J.; Gwyther, J.; Hudson, Z. M.; Kynaston, E.; Rupar, P. A.; Winnik, M. A.; Manners, I. *J. Am. Chem. Soc.* **2014**, *136*, 4121−4124. (c) He, W. N.; Xu, J. T. *Prog. Polym. Sci.* **2012**, *37*, 1350−1400. (d) Qi, H.; Wang, W. D.; Li, C. Y. *ACS Macro Lett.* **2014**, *3*, 675−678. (e) Wang, W. D.; Li, C. Y. *ACS Macro Lett.* **2014**, *3*, 175−179. (f) Wang, H. W.; Pentzer, E.; Emrick, T.; Russell, T. P. *ACS Macro Lett.* **2014**, *3*, 30−34. (g) Sun, J.; Teran, A. A.; Liao, X. X.; Balsara, N. P.; Zuckermann, R. N. *J. Am. Chem. Soc.* **2014**, *136*, 2070−2077. (h) Pitto-Barry, A.; Kirby, N.; Dove, A. P.; O'Reilly, R. K. *Polym. Chem.* **2014**, *5*, 1427−1436. (i) Hammer, B. A. G.; Reyes-Martinez, M. A.; Bokel, F. A.; Liu, F.; Russell, T. P.; Hayward, R. C.; Briseno, A. L.; Emrick, T. *ACS Appl. Mater. Interfaces* **2014**, *6*, 7705−7711.
(10) Wang, H. P.; Keum, J. K.; Hiltner, A.; Baer, E.; Freeman, B.; Rozanski, A.; Galeski, A. *Science* **2009**, *323*, 757−760.
(11) (a) Liang, G. D.; Weng, L. T.; Lam, J. W. Y.; Qin, W.; Tang, B. *ACS Macro Lett.* **2014**, *3*, 21−25. (b) Liang, G. D.; Xu, J. T.; Fan, Z. Q.; Mai, S. M.; Ryan, A. J. *Macromolecules* **2006**, *39*, 5471−5478. (c) Su, M.; Huang, H. Y.; Ma, X. J.; Wang, Q.; Su, Z. H. *Macromol. Rapid Commun.* **2013**, *34*, 1067−1071.
(12) (a) Delcorte, A. In *ToF-SIMS: Materials Analysis by Mass Spectrometry*, 2nd ed.; Vickerman, J. C., Briggs, D., Eds.; IM Publications and Surface Spectra Limited: Chichester, 2013; pp 87−123. (b) Weng, L. T.; Chan, C. M. In *ToF-SIMS: Materials Analysis by Mass Spectrometry*, 2nd ed.; Vickerman, J. C., Briggs, D., Eds.; IM Publications and Surface Spectra Limited: Chichester, 2013; pp 87−123. (c) Weng, L. T.; Chan, C. M. In *Wiley Encyclopedia of Composites*, 2nd ed.; Nicolais, L., Borzacchiello, A., Lee, S. M., Eds.; Wiley: Chichester, 2012; pp 2974−2993.
(13) (a) Bao, S. P.; Qin, W. P.; Wu, Q. H.; Liang, G. D.; Zhu, F. M.; Wu, Q. *Dalton Trans.* **2013**, *42*, 5242−5246. (b) Bao, S. P.; Liu, T. T.; Liang, G. D.; Gao, H. Y.; Zhu, F. M.; Wu, Q. *Chem.—Eur. J.* **2012**, *18*, 15272−15276.
(14) Hu, H. L.; Dorset, D. L. *Macromolecules* **1990**, *23*, 4604−4607.
(15) (a) Wang, B. B.; Li, B.; Zhao, B.; Li, C. Y. *J. Am. Chem. Soc.* **2008**, *130*, 11594−11595. (b) Cheng, S. Z. D.; Wu, S. S.; Chen, J. H.; Zhuo, Q. H.; Quirk, R. P.; Vonmeerwall, E. D.; Hsiao, B. S.; Habenschuss, A.; Zschack, P. R. *Macromolecules* **1993**, *26*, 5105−5117.
(16) (a) Liang, G. D.; Wu, Q. H.; Qin, W. P.; Bao, S. P.; Zhu, F. M.; Wu, Q. *Polym. Chem.* **2013**, *4*, 3821−3828. (b) Liang, G. D.; Wu, Q. H.; Bao, S. P.; Zhu, F. M.; Wu, Q. *Polym. Chem.* **2013**, *4*, 5671−5678.

DOI: 10.1021/acsmacrolett.5b00180
ACS Macro Lett. 2015, 4, 593−597